Progress In Electromagnetics Research C, Vol. 80, 211–219, 2018

Experimentally Validated, Wideband, Compact, OAM Antennas Based on Circular Vivaldi Antenna Array

Tianming Yang*, Deqiang Yang, Boning Wang, and Jianzhong Hu

Abstract—The bandwidth of OAM antennas, which have a great potential for multiple-input multiple-output (MIMO) communication, must be wide enough. Unfortunately, most of researchers only care about the generation and characteristics of vortex beams carrying orbital angular momentum (OAM) but ignore the bandwidth of OAM antennas. To develop OAM antenna suitable for MIMO communication, Vivaldi antenna is used as the element of circular array because of its wide bandwidth. Three compact wideband circular Vivaldi antenna arrays that can generate vortex beams carrying OAM with numbers of modes $l = 0, -2, +2$ are proposed and experimentally validated in this paper. Measured results show that the proposed antennas can radiate vortex beams with different numbers of modes over a frequency range of 2.7–2.9 GHz.

1. INTRODUCTION

Electromagnetic wave can carry not only energy, but also angular momentum which is composed of spin angular momentum (SAM) and OAM [1]. Circular polarized beams, which are electromagnetic beams carrying SAM, only have two orthogonal modes which are known as left-hand and right-hand circular polarizations. Vortex beams, which can propagate along the transverse direction, are electromagnetic beams carrying different orthogonal OAMs with unlimited numbers of modes $l = 0, \pm1, \pm2 \ldots$. Therefore, vortex beams with different OAM modes have great potential to improve transmission capacity and spectrum efficiency in wireless communications, and can be used for multiplexing in free-space communication [2]. Besides, OAM beams also have a great potential for radar target recognition and imaging because of the spiral phase structure distribution of them [3].

Recently, several antennas for generating vortex beams carrying OAM in radio frequency have been proposed: (i) traveling-wave ring-slot antennas [4–6], (ii) circular antenna arrays [7, 8], (iii) circular leaky-wave antenna [9], (iv) helicoidal parabolic antenna [10], (v) Circular polarized patch antenna [11]. Although the antennas reported in [4–11] can generate vortex beams with helical phase fronts successfully, their bandwidth, which is always not mentioned, is usually narrow which makes them not suitable for wideband wireless communication. The relative impedance bandwidths of the antennas in [4, 7, 11] are less than 0.2%, 1% and 0.6%, respectively. Thus, Vivaldi antenna is adopted as array element of circular antenna array to generate OAM over a wide frequency range of 2.7–2.9 GHz (7.1%) in this paper.

Although the researchers have generated OAM radio waves using circular Vivaldi antenna array in [8], they just gave the simulated results, did not integrate the antenna array with feed network and failed to distinguish the number of OAM modes by the phase patterns. In this work, a Vivaldi antenna array is integrated with a feed network, thus the wide bandwidth of the antenna array is preserved in the whole set. Besides, to obtain the phase patterns in the near-field zone, two independent polarization components $\overrightarrow{E}x$ and $\overrightarrow{E}y$ are measured due to different polarized directions of the element antennas.

Received 7 November 2017, Accepted 10 January 2018, Scheduled 23 January 2018

* Corresponding author: Tianming Yang (tmy_uestc@163.com).
The authors are with the School of Electronic Engineering, University of Electronic Science and Technology of China, Chengdu, Sichuan, China.

2. MATHEMATICAL MODEL OF THE ANTENNA ARRAY

As shown in [12], a circular antenna array with N equidistant elements can generated vortex beams carrying OAM with number of modes l when the elements are fed with signal with the same amplitude, but with $2\pi l/N$ phase difference between adjacent elements. For generality, it is assumed that each antenna element consists of a tripole [12]. However, the antenna array factor will be different if the antenna elements are dipoles when the dipoles are arranged along a circumference as shown in Figure 1.

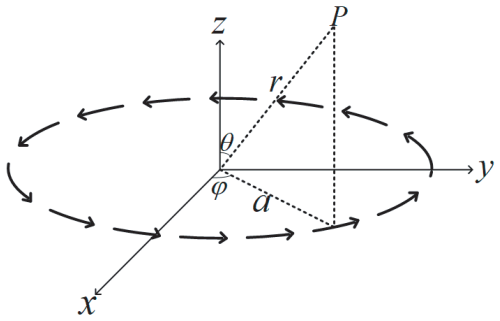

Figure 1. Mathematical model of a circular antenna array.

The current distribution of the nth element in Figure 1 is $\widehat{J}(n) = \widehat{\varphi} I_0 e^{-jl\varphi_n}$, where $\varphi_n = 2\pi n/N$ is the azimuth position of the nth element, and I_0 is the constant current density. $a = |r_n|$ denotes the radius of the array. Thus, a circular array's vector potential can then be described as

$$\begin{aligned}
\overrightarrow{A}(\widehat{r}) &= \frac{\mu I_0}{4\pi} \sum_{n=1}^{N} e^{-jl\varphi_n} \int \frac{e^{-jk|r-r'_n|}}{|r-r'_n|} dV'_n \\
&= \frac{\mu I_0}{4\pi} \sum_{n=1}^{N} e^{-jl\varphi_n} \frac{e^{-jk|r-r'_n|}}{|r-r'_n|} a d\phi' \\
&\approx \frac{\mu a I_0 e^{-jkr}}{4\pi r} \sum_{n=1}^{N} e^{j(k\cdot r_n - l\varphi_n)} d\phi' \qquad (1)
\end{aligned}$$

Here, the standard infinitesimal dipole approximation $|\widehat{r} - \widehat{r}_n| \approx r - \widehat{r} \cdot \widehat{r}_n$ for phases and $|\widehat{r} - \widehat{r}_n| \approx r$ for amplitudes is used [13]. If N is sufficiently large, the vector potential can be approximated by integral over the angle φ_n

$$\begin{aligned}
\overrightarrow{A}(\widehat{r}) &\approx \frac{\mu a I_0 e^{-jkr}}{4\pi r} \int_0^{2\pi} e^{-jl\varphi'} e^{jka\sin\theta\cos(\varphi-\varphi')} \left(-\widehat{x}\sin\varphi' + \widehat{y}\cos\varphi'\right) d\varphi' \\
&= \frac{j^{-l}\mu a I_0 e^{-jkr} e^{-jl\varphi}}{4r} \left[\left(\widehat{r}\sin\theta + \widehat{\theta}\cos\theta - \widehat{\varphi} j\right) J_{l-1}(ka\sin\theta) \right. \\
&\quad \left. + \left(\widehat{r}\sin\theta + \widehat{\theta}\cos\theta + \widehat{\varphi} j\right) J_{l+1}(ka\sin\theta) \right] \\
&= \frac{j^{-l}\mu a I_0 e^{-jkr} e^{-jl\varphi}}{4r} \left[\left(\widehat{r}\sin\theta + \widehat{\theta}\cos\theta\right) \frac{2l}{ka\sin\theta} J_l(ka\sin\theta) - \widehat{\varphi} j 2 J'_l(ka\sin\theta) \right] \qquad (2)
\end{aligned}$$

According to the conventional electromagnetic theories, the electric fields can be obtained based on the vector potential $\overrightarrow{A}(\widehat{r})$

$$\overrightarrow{E}(\widehat{r}) = -j\omega \overrightarrow{A}(\widehat{r}) \qquad (3)$$

$$E_\varphi(\widehat{r}) = \frac{j^{-l+1}\omega\mu a I_0 e^{-jkr} e^{-jl\varphi}}{2r} J'_l(ka\sin\theta) \qquad (4)$$

Clearly, the electric field for this circular antenna array has the azimuth dependency of $e^{-jl\varphi}$, which is the general characteristic of the vortex beams. Note the derivative of the first kind Bessel function $J_l'(ka\sin\theta)$. E_φ will be equal to zero when θ is equal to zero, and l is not equal to ± 1. Thus, the electric field density of the vortex beams is zero along the z axis except the vortex beam carrying OAM with number of modes ± 1.

3. DESIGN OF THE CIRCULAR ANTENNA ARRAY

Figures 2(a) and 2(b) show the top and bottom views of the element Vivaldi antennas. Their substrate is FR4. Its relative permittivity is 4.4; thickness is 0.8 mm; the thickness of its electrodeposited copper is 35 µm. On the top layer of the substrate, a pair of symmetrical resonant structures, which can add the lower resonator frequency, sprout from the ground plane to reduce the size of the transverse dimensions. The profile of the exponential curve E_1 can be described by

$$E_1 : x = \begin{cases} C_1 \exp(ay) + C_2, & (0 \le y \le H, x > 0) \\ -(C_1 \exp(ay) + C_2), & (0 \le y \le H, x < 0) \end{cases} \tag{5}$$

where a and H are equal to 0.17 and 27, respectively, and C_1 and C_2 can be defined as:

$$\begin{aligned} C_1 &= \frac{y_2 - y_1}{\exp(ax_2) - \exp(ax_1)} \\ C_2 &= \frac{y_2 \exp(ax_2) - y_1 \exp(ax_1)}{\exp(ax_2) - \exp(ax_1)} \end{aligned} \tag{6}$$

where (x_1, y_1) and (x_2, y_2) are the start and end points of the exponential tapered curve, respectively, and x_1, y_1, x_2, and y_2 are equal to 0.3, 0,15, and 27, respectively.

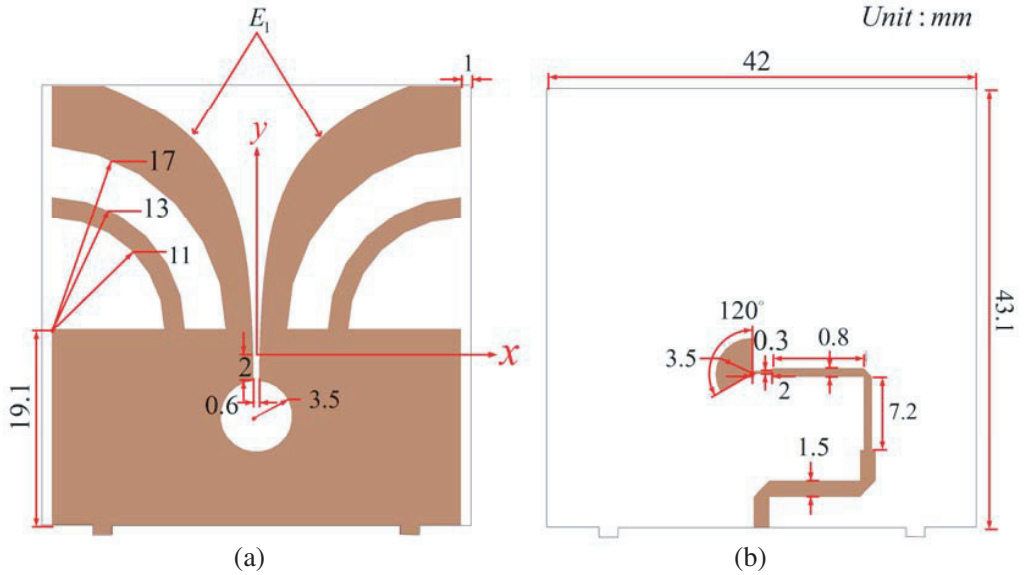

Figure 2. Geometry of the element Vivaldi antennas. (a) Top view. (b) Bottom view.

Then, eight miniaturized Vivaldi antenna elements are folded into a hollow regular octagon as shown in Figure 3. The regular octagon's radius R is equal to $W/\sin(\pi/8)/2$ (54.9 mm), where W is equal to 42 mm. R is approximately equal to $0.51\lambda_c$, and λ_c, which is the operating wavelength at the central frequency (2.8 GHz) of the antenna array, is approximately equal to 107.6 mm. Like the typical circular antenna array [14], elements of the proposed antennas are fed with signals with the same amplitude, but with $2\pi l/N$ phase difference between adjacent elements, where N is the number of the elements of the array, and l is number of modes. Thus, there are phase changes $2\pi l$ around a closed circle perpendicular to the propagation direction. Thus, the proposed antenna arrays can generate OAM

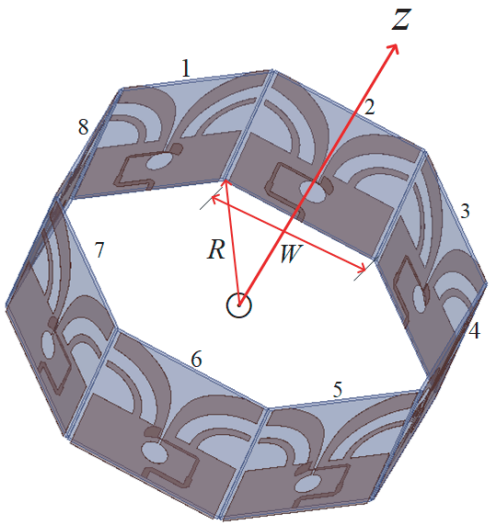

Figure 3. Circular Vivaldi antenna array.

beams with number of modes 0, −2, +2 by changing the phase difference between adjacent elements at the gradients of 0°, −90°, +90°, respectively.

The classical topologies of the feed networks, which consist of 3 dB Wilkinson power dividers, 90° and 180° hybrid couplers, are given in Figure 4. The phase difference between output ports of the feed networks in Figures 4(a) and 4(b) are 0°, −90°, respectively. The classical topology of the feed networks with 90° phase difference between adjacent outputs is basically the same as Figure 4(b). The only difference is that the output port is in reverse order.

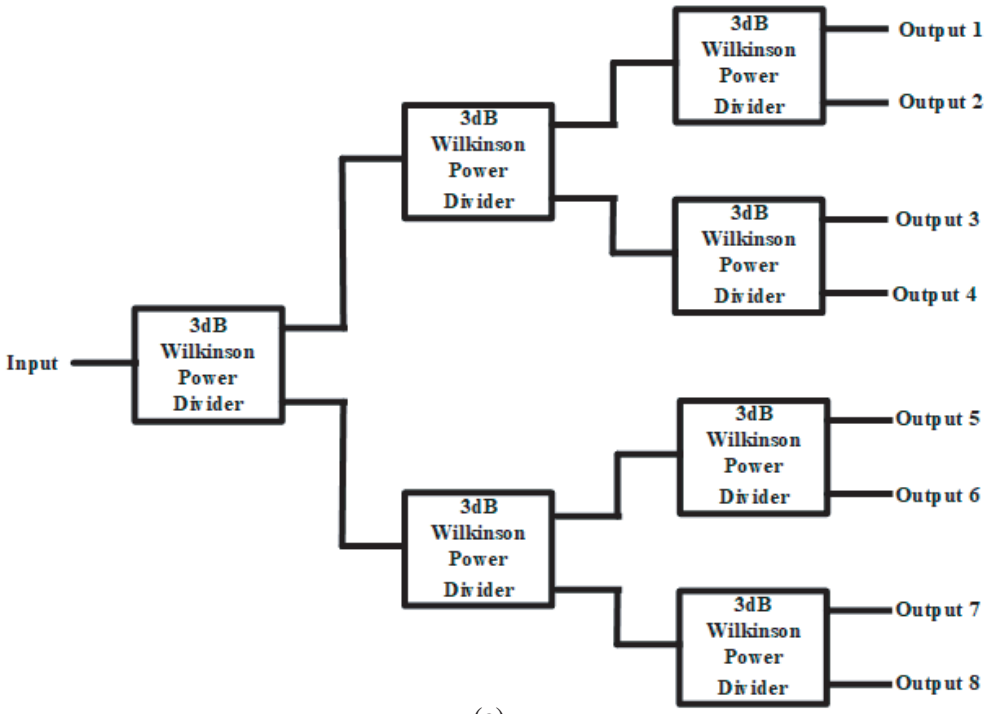

(a)

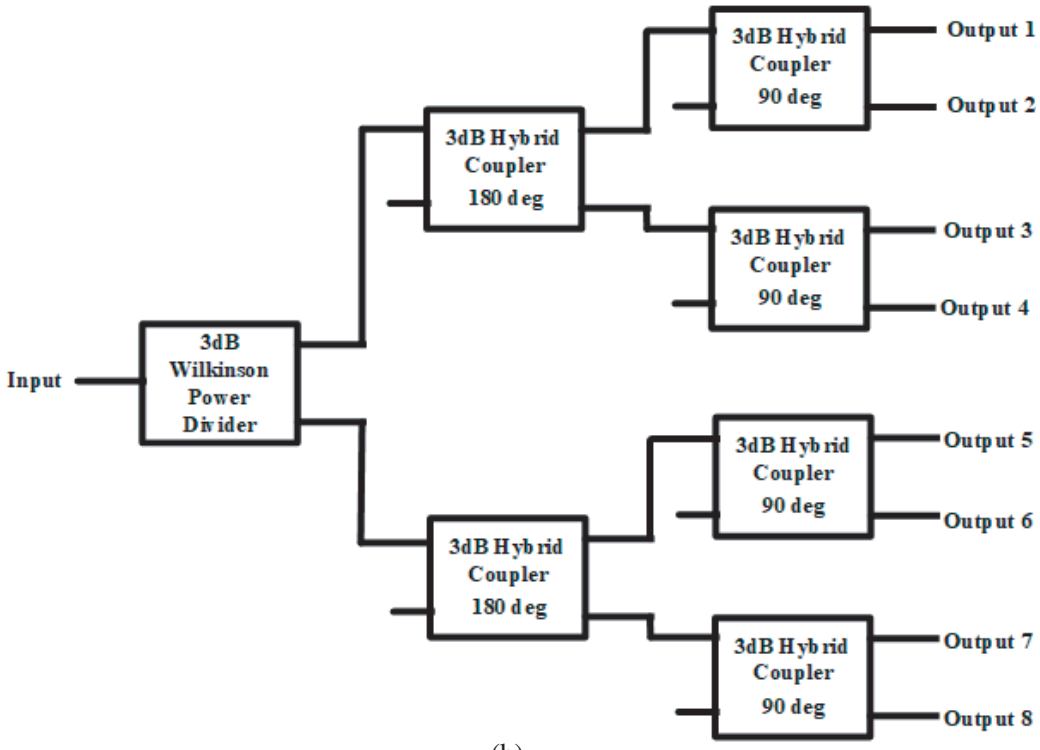

(b)

Figure 4. The classical topology of the feed networks. (a) 0° phase gradient. (b) −90° phase gradient.

4. EXPERIMENTAL DEMONSTRATION

Three pairs of antenna array prototypes, shown in Figure 5, are fabricated and then measured. The scattering parameters of the antennas are measured by a vector network analyzer (Agilent N9912A), and its phase pattern in the nearfield is measured in a 25 m × 15 m × 15 m microwave chamber at the University of Electronic Science and Technology of China. The reflection coefficient of the three antenna arrays together with the Vivaldi antenna element are shown in Figure 6, and Figure 7 shows the measurement step of the transmission coefficient between different antenna arrays. The distance

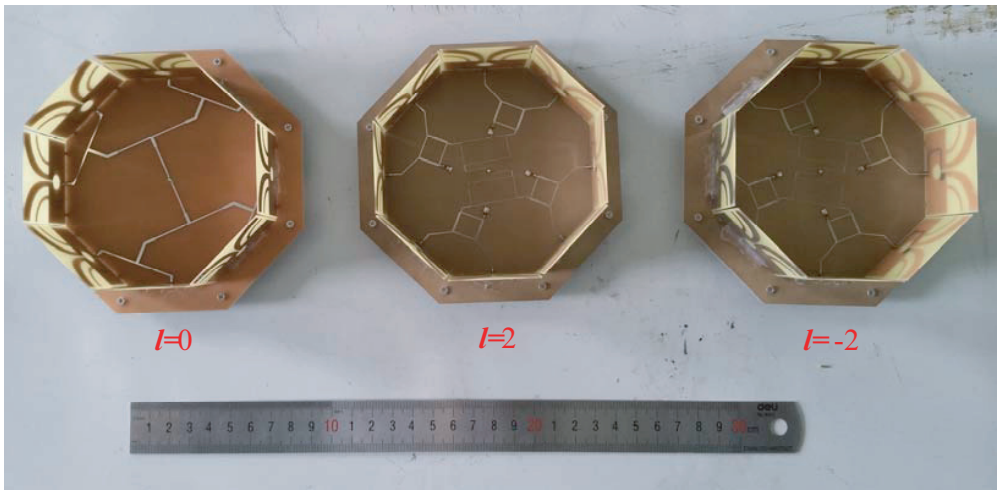

Figure 5. Antenna array prototypes.

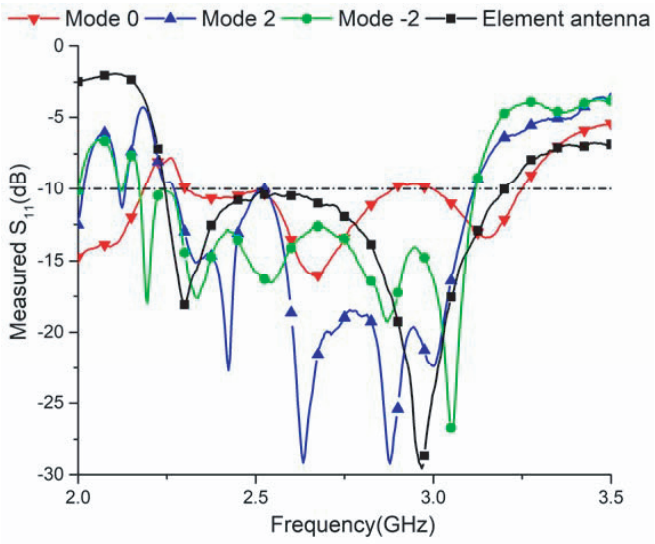

Figure 6. Measured reflection coefficient.

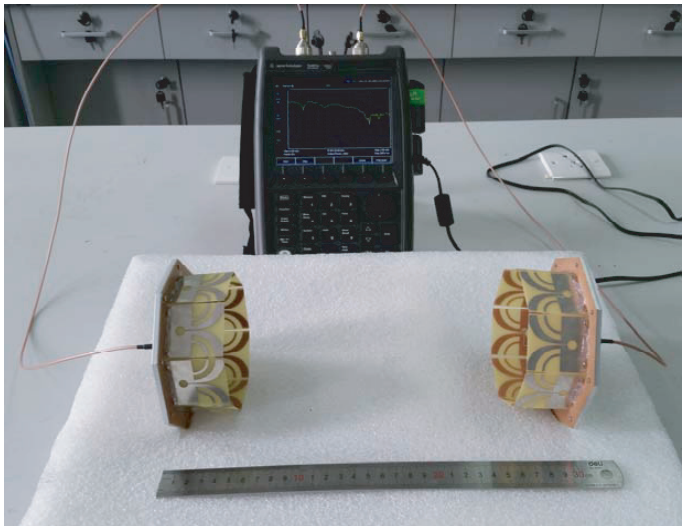

Figure 7. Measurement setup.

between two antenna arrays to be measured is equal to $2\lambda_c$ approximately. Figure 8 gives the measured results of the transmission coefficient when the frequency varies from 2.7–2.9 GHz. The results show that the transmission coefficients between two antenna arrays with the same number of modes are about 10 dB higher than two antenna arrays with different numbers of modes, which means that the antenna arrays with different numbers of modes are mutually independent.

The near-field phase patterns at the operating frequencies of 2.7, 2.8 and 2.9 GHz are measured by a vector network analyzer and an open-end rectangular waveguide probe. The measurement setup of the near-field phase pattern is shown in Figure 9. The distance between antenna aperture and the probe z_o is about $2\lambda_c$, and the transverse electric field of $0.6 \times 0.6\,\mathrm{m}^2$ is measured successfully. Two independent polarization components $\overrightarrow{E}_x$ and $\overrightarrow{E}_y$ are measured due to different polarized directions of the element antennas. The phase patterns of the electric field component $\overrightarrow{E}_\varphi$ in the measured transverse near-field plane, which is calculated from the Cartesian components as $\overrightarrow{E}_\varphi = \overrightarrow{e}_\varphi(-E_x \sin\varphi + E_y \cos\varphi)$, are shown in Table 1. The results show that there are phase changes $2\pi l$ around a closed circle perpendicular to the propagation direction over a frequency range of 2.7–2.9 GHz.

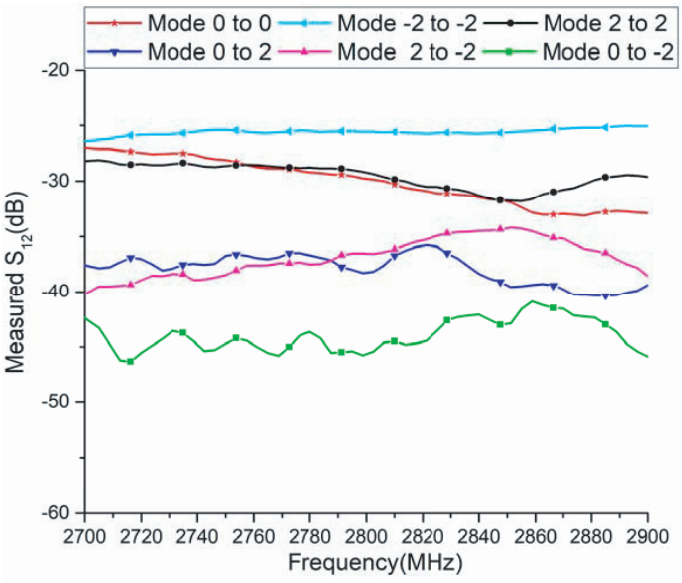

Figure 8. Measured transmission coefficient.

Table 1. The near-field phase patterns of the antenna arrays with different modes at different frequencies.

	f=2.7 GHz	*f*=2.8 GHz	*f*=2.9 GHz
l=0	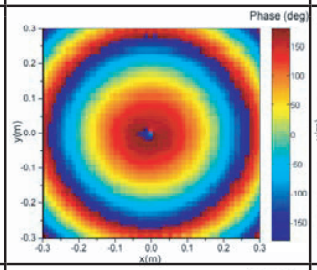	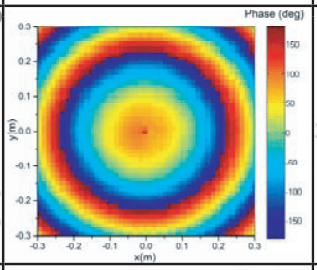	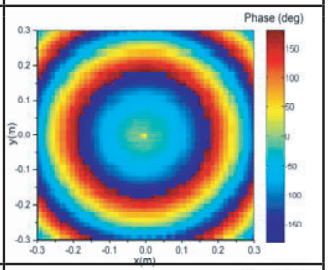
l=-2	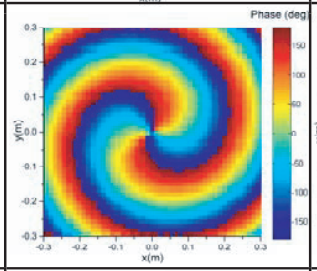	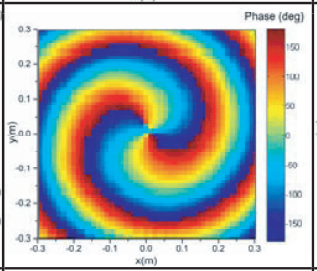	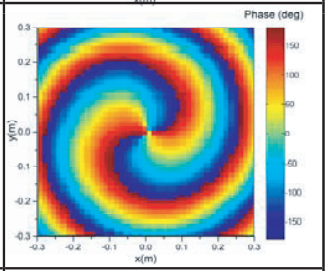
l=2	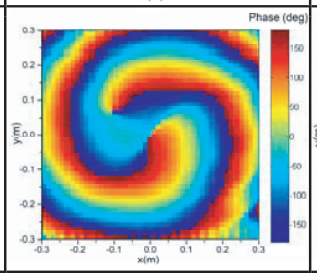	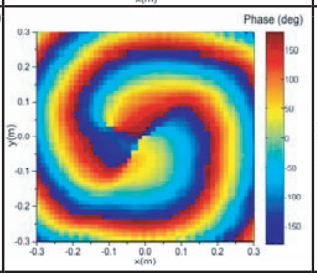	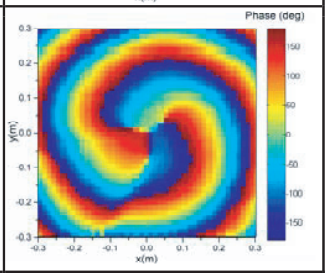

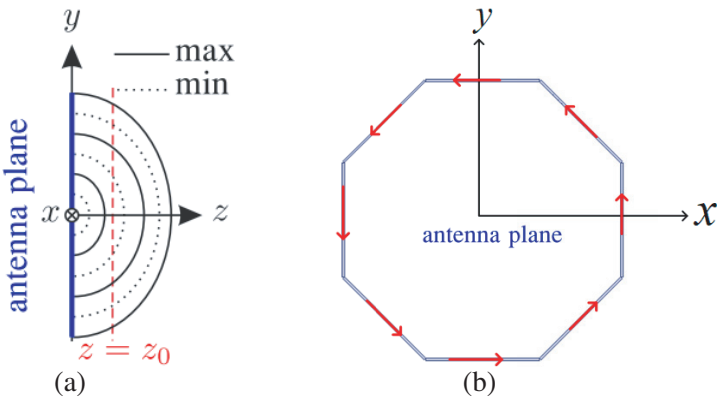

Figure 9. Measurement setup of the near-field radiation pattern. (a) Configuration of the scanning platform. (b) The antenna plane.

5. CONCLUSION

Three compact wideband circular Vivaldi antenna arrays that can generate vortex beams carrying OAM over a frequency range of 2.7–2.9 GHz with numbers of modes $l = 0, -2, +2$ are proposed and experimentally validated in this paper. To obtain the phase of the electric field component $\overrightarrow{E}_{\varphi}$, two independent polarization components $\overrightarrow{E}_x$ and $\overrightarrow{E}_y$ are measured. Measured results including the transmission coefficients between two antenna arrays and the near-field phase patterns confirm that the antenna arrays with different numbers of modes are mutually independent.

REFERENCES

1. Allen, L., M. W. Beijersbergen, R. J. Spreeuw, and J. P. Woerdman, "Orbital angular momentum of light and the transformation of Laguerre-Gaussian laser modes," *Phys. Rev. A, Gen. Phys.*, Vol. 45, No. 11, 8185, 1992.
2. Zhang, W., S. Zheng, X. Hui, R. Dong, X. Jin, H. Chi, and X. Zhang, "Mode division multiplexing communication using microwave orbital angular momentum: An experimental study," *IEEE Transactions on Wireless Communications*, Vol. 16, 1308–1318, 2017.
3. Chen, Y., S. Zheng, X. Jin, H. Chi, and X. Zhang, "Single-frequency computational imaging using OAM-carrying electromagnetic wave," *Journal of Applied Physics*, Vol. 121, 6–43, 2017.
4. Zhang, W., S. Zheng, X. Hui, Y. Chen, X. Jin, H. Chi, and X. Zhang, "Four-OAM-mode antenna with traveling-wave ring-slot structure," *IEEE Antennas and Wireless Propagation Letters*, Vol. 16, 194–197, 2017.
5. Zhang, Z., S. Zheng, X. Jin, H. Chi, and X. Zhang, "Generation of plane spiral OAM waves using traveling-wave circular slot antenna," *IEEE Antennas and Wireless Propagation Letters*, Vol. 16, 8–11, 2016.
6. Mao, F., M. Huang, T. Li, J. Zhang, and C. Yang, "Broadband generation of orbital angular momentum carrying beams in RF regimes," *Progress In Electromagnetics Research*, Vol. 160, 19–27, 2017.
7. Choi, J. and S. Oh, "Design of a circular array antenna for generating waves with orbital angular momentum," *Microwave and Optical Technology Letters*, Vol. 59, No. 9, 2246–2249, 2017.
8. Deng, C., W. Chen, Z. Zhang, Y. Li, and Z. Feng, "Generation of OAM radio waves using circular Vivaldi antenna array," *International Journal of Antennas and Propagation*, Vol. 2013, Article ID 847859, 7 pages, 2013.
9. Al-Bassam, A., M. A. Salem, and C. Caloz, "Vortex beam generation using circular leaky-wave antenna," *Antennas and Propagation Society International Symposium*, 1792–1793, 2014.

10. Mari, E., F. Spinello, M. Oldoni, R. A. Ravanelli, F. Romanato, and G. Parisi, "Near-field experimental verification of separation of OAM channels," *IEEE Antennas and Wireless Propagation Letters*, Vol. 14, 556–558, 2015.
11. Barbuto, M., F. Trotta, F. Bilotti, and A. Toscano, "Circular polarized patch antenna generating orbital angular momentum," *Progress In Electromagnetics Research*, Vol. 148, 23–30, 2014.
12. Mohammadi, S. M., L. K. S. Daldorff, J. E. S. Bergman, R. L. Karlsson, T. Bo, K. Forozesh, T. D. Carozzi, and B. Isham, "Orbital angular momentum in radio — A system study," *IEEE Transactions on Antennas and Propagation*, Vol. 58, 565–572, 2010.
13. Courtial, J., D. A. Robertson, K. Dholakia, L. Allen, and M. J. Padgett, "Rotational frequency shift of a light beam," *Physical Review Letters*, Vol. 81, 4828–4830, 1998.
14. Gong, Y., R. Wang, Y. Deng, B. Zhang, N. Wang, N. Li, and P. Wang, "Generation and transmission of OAM-carrying vortex beams using circular antenna array," *IEEE Transactions on Antennas and Propagation*, Vol. 65, No. 6, 2940–2949, 2017.